Transport and Ion Exchange in Langmuir-Blodgett Films: Water Transport and Film Microstructure by Attenuated Total Reflectance Fourier Transform Infrared Spectroscopy

Tracy L. Marshbanks,† Dong June Ahn, and Elias I. Franses*

School of Chemical Engineering, Purdue University, West Lafayette, Indiana 47907-1283

Received July 16, 1993. In Final Form: October 1, 1993®

Langmuir-Blodgett (LB) films of calcium stearate were studied by FTIR before, during, and after contact with water and aqueous solutions of hydrochloric acid. The films retain from 1.5 to 3 wt % water of hydration, and they absorb at least 8 wt % (possibly up to 16 wt %) water, probably in voids, when contacted with bulk liquid water. The effective diffusivity of water in the films was estimated from the data to be in the range from about 10^{-13} to 10^{-10} $cm^2 \cdot s^{-1}$, but water transport was probably neither purely diffusive nor one-dimensional. The effects of ion exchange and thermal annealing at 100–140 °C on the film microstructure was monitored by detailed analysis of polarized ATR spectra. Conversion of calcium stearate to stearic acid caused film dehydration, recrystallization, and an increase in trans conformations. Certain implications on the barrier, transport, and ion exchange properties of LB films are discussed.

1. Introduction

LB films have been studied extensively in the past 15 years for their potential importance as materials for thin barriers, membranes, and optical applications.[1-3] Because the film quality is important for these applications, many workers have reported on the use of various microscopic and spectroscopic techniques for probing pinholes, defects, grain boundaries, etc.[1-4] Little is known, however, on how these defects affect the overall transport properties of LB films.

Calcium stearate has been chosen for study, because it readily forms stable, crystalline, and well-characterized LB films.[5,6] This paper focuses on measuring the transport rate of water, because it is important for barrier or membrane applications, and also because it may provide an overall measure of the film microstructure and quality. The film microstructure is also probed by attenuated total reflectance Fourier transform infrared (ATR-FTIR) spectroscopy before and after ion exchange of Ca^{2+} by H^+. The ion exchange dynamics results for the same systems have been obtained and will be reported later.

2. Experimental Section

2.1. Materials. Stearic acid (puriss grade, 99%), calcium chloride dihydrate (purum grade, > 99%), and hydrochloric acid were purchased from Fluka Chemical Co. The sulfuric and acetic acids were of reagent grade and were obtained from Fisher Scientific. All water used was purified using a Mili-Q four-bowl system, from Millipore Corp., and had an initial resistivity of 18 MΩ/cm. The germanium internal reflection plates were purchased from Harrick Scientific and Wilmad Glass Co.; they were 50 × 10 × 2 mm trapezoids with 45° angle faces.

2.2. Apparatus and Procedures. The Langmuir trough was a MiniTrough-4 purchased from Joyce-Loebl of Gateshead, England. The trough used a Wilhelmy paper plate for measuring surface tension and a continuous constant-perimeter Teflon barrier for film containment. The trough was housed in a clean room equipped with a laminar flow hood.

The subphase calcium ion concentration ($CaCl_2$) was 1×10^{-4} M, and NH_4OH was added to control the subphase pH to 8. The surface was cleaned by pipette suction until there was no detectable surface pressure upon maximum area compression. Sufficient stearic acid was spread from droplets of a 1 mg/mL hexane solution, to provide an initial area of 40 $Å^2$ per molecule. The film compression was started 15 min after the surfactant spreading to allow for the hexane to evaporate completely. All depositions were conducted at a surface pressure of 25 mN/m. The film was held at this pressure for 10 min prior to the start of the deposition. This allowed for the film to stabilize prior to the film transfer procedure. The transfer ratio ranged from 0.95 to 1.0.

The ATR plates were cleaned by first washing with a detergent solution, followed by rinsing in deionized water, ethyl alcohol, and water again. The crystal was then cleaned in a Harrick Scientific PDC-3XG cleaner/sterilizer, first in an oxygen plasma for 5 min and then for 5 min in an argon plasma. The final step in the cleaning procedure was a Millipore water rinse. This cleaning procedure produced substrates which consistently yielded uniform film disposition, if they were still coated by a water film. Deposition onto dried crystals resulted in poor quality films which had lateral striations.

Infrared spectra were collected with a Nicolet System 800 FTIR spectrometer. The optical bench was equipped with a DTGS room temperature detector and a narrow band MCT-A cryogenic detector. The removal beamsplitter was constructed of Ge and KBr. The instrument was continually purged with dry air from a Balston air purifier. The bench was equipped with an internal, computer-controlled, wire-grid, polarizer. The ATR optics for the System 800 spectrometer were custom-built by Connecticut Instruments, Inc. This accessory held the crystal face at a horizontal position and was capable of angles of incidence from 30° to 60°.

A sample chamber which fit on the ATR top crystal surface was constructed (Figure 1). This chamber allowed liquid to contact the LB film covering the top side of the ATR element. The LB film on the bottom side of the ATR crystal was removed, to enhance the sensitivity of the experiment to the transport and reaction occurring on the upper surface and to simplify the

* Author to whom correspondence should be addressed, telephone (317) 494-4078.

† Present address: Amoco Oil, Amoco Research Center, P.O. Box 3011, Naperville, IL 60566-7011.

® Abstract published in *Advance ACS Abstracts,* November 15, 1993.

(1) Stroeve, P., Franses, E. I., Eds. *Molecular Engineering of Ultrathin Polymeric Films*; Elsevier: London, 1987, also *Thin Solid Films* **1987**, *152* (1, 2).

(2) Petty, M. C. In *Langmuir-Blodgett Films*; Roberts, G. G., Ed.; Plenum Press: New York, 1990; p 133.

(3) Ulman, A. *An Introduction to Ultrathin Organic Films. From Langmuir-Blodgett to Self-Assembly*; Academic Press: New York, 1991.

(4) Lesieur, P.; Barraud, A.; Vandevyver, M. *Thin Solid Films* **1987**, *152*, 155.

(5) Takenaka, T.; Nogami, K.; Gotoh, H.; Gotoh, R. *J. Colloid Interface Sci.* **1971**, *35*, 395.

(6) Kimura, F.; Umemura, J.; Takenaka, T. *Langmuir* **1986**, *2*, 96.

0743-7463/94/2410-0276$04.50/0

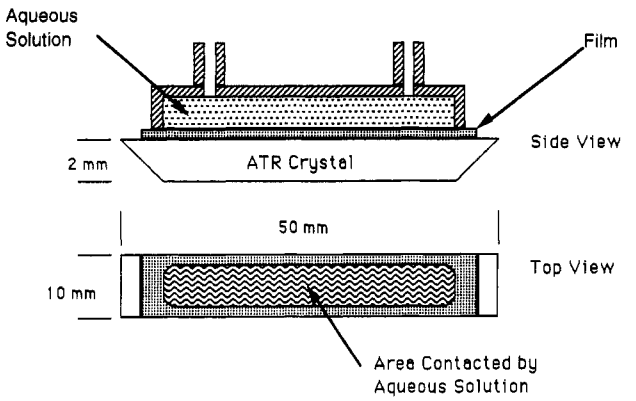

Figure 1. Schematic of ATR assembly used for water and ion transport studies.

spectral analysis by removing spectral features due to film not contacted by the aqueous solution. After the sample was mounted, high-resolution (1 cm^{-1}) spectra at 0° (s) and 90° (p) polarizations were collected, followed by a low-resolution (8 cm^{-1}) spectrum for reference. The aqueous solution was then injected onto the film and infrared spectra were collected at short time intervals to follow the dynamics within the LB film. Normally, an 8-cm^{-1} spectrum of a good S/N ratio could be collected in about 2 s, which provides good time-resolved spectra of the film dynamics. After the transport process was completed, the solution was removed, the sample was dried in the dry instrument atmosphere, and another set of high-resolution, polarized spectra was collected. The ATR crystal was then cleaned and the various background spectra were collected. Certain LB films were annealed in a laboratory oven. Spectra were fit by using a nonlinear least-squares algorithm. The analysis also provided estimates for the fit parameters.

Results and Discussion

3.1. Film Microstructure before and after Water Contact. A 119-layer film was used for estimating the water solubility and the rate of water uptake in LB films of dried $CaSt_2$. A relatively thick LB film was required to decrease the ATR-infrared signal of the overlying water and to increase the total amount of water uptake in the film. It would take a much thicker film (>3 μm) to totally eliminate the signal from the overlying water. Spectra were collected before and after the water contact, in order to probe any structural changes within the film. Figure 2 shows various regions of the spectrum at 0° polarization. At 90° polarization, the spectrum is about the same with some differences in the relative peak intensities, due to the dichroism of various vibrations.[7] Peaks are identified in Table I. A detailed analysis of the entire spectra and fitting of the hydrocarbon stretch region were done, in order to find the water of hydration, the initial microstructure of the film, and any possible changes in the crystal structure or orientation upon water contact.

There was some water in the film, prior to contact with water, as indicated by the broad peaks centered around 3560 and 3380 cm^{-1} (Figure 2). When water was placed directly on the ATR plate and when water was placed on the LB film, there was only one broad peak, centered at 3380 cm^{-1}. It appears that the water in the dried film is water of hydration, although the amount is not the same after further exposure to water and subsequent drying. The integrated absorbances, from 3800 to 3000 cm^{-1}, before and after exposure to water are A_{H0} = 9.5 cm^{-1} and A_{Hf} = 4.1 cm^{-1}, respectively. The decrease is probably due either to drying in the low-humidity (purged) bench or to dissolution by water of traces of calcium salt, which may have been entrained and which is hygroscopic.

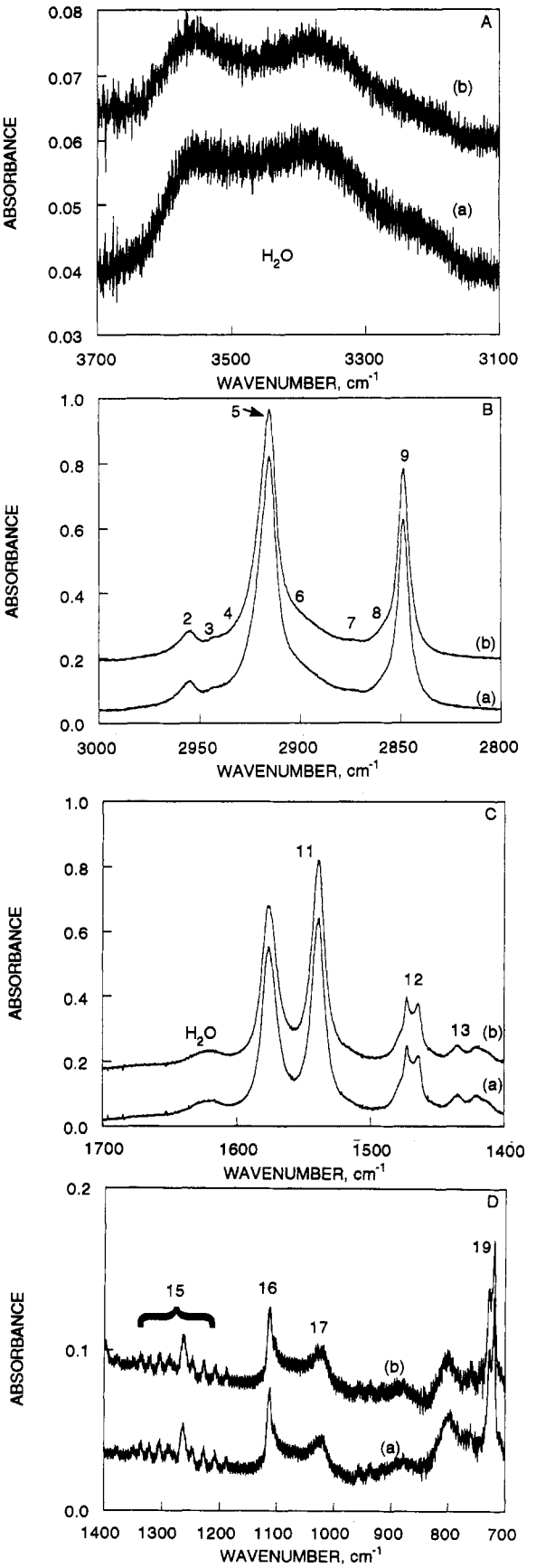

Figure 2. Polarized (0°) ATR spectra of a 119-layer LB film of $CaSt_2$ on Ge before (a) and after (b) exposure to water. 1 cm^{-1} resolution. A, B, C, and D are different spectral regions; for peak assignments see Table I.

(7) Marshbanks, T. L. Ph.D. Thesis, Purdue University, West Lafayette, IN, 1992.

Table I. Peak Assignments for StH and $CaSt_2$ LB Films

peak	vibration	comment
1	CH_3 ν_a i.p.	methyl asymmetric stretch, in backbone plane
2	CH_3 ν_a o.p.	methyl asymmetric stretch, out of backbone plane
3		appears in $CaSt_2$, α-CH_2, COO^- overtone
4	CH_3 ν_s	Fermi resonance
5	CH_2 ν_a	methylene asymmetric stretch
6	CH_2 ν_s	Fermi resonance
7	CH_3 ν_s	methyl symmetric stretch
8		CH_2 ν_s, α-methylene
9	CH_2 ν_s	methylene symmetric stretch
10	C=O ν	carbonyl stretch
11	COO^- ν_a	carboxylate asymmetric stretch
12	CH_2 δ	methylene scissor
13	COO^- ν_s	carboxylate symmetric stretch
14	COOH	O–C–O–H deformation
15	CH_2 $\omega + \gamma$	progression band
16		COO^- deformation, OH deformation
17	C–C	carbon–carbon vibration
18	OH deform. o.p.	O–H out-of-plane deformation
19	CH_2 r	methylene chain totally in-phase rock

The above absorbances can be used to quantitatively estimate the water density in the film, by using well-established ATR theory, as follows. The electric field amplitude of the evanescent wave decays exponentially with distance x from the plate–film interface. The absorbance depends of course on the square of the amplitude. Then[8-10]

$$A_{H0} = \int_0^l \rho_{wf}^{\circ}\alpha_{wf}\, e^{-2\gamma_f x}\, dx = \frac{\rho_{wf}^{\circ}\alpha_{wf}}{2\gamma_f}(1 - e^{-2\gamma_f l}) \quad (1)$$

Here ρ_{wf}° is the molar density (presumed uniform) of water in the film, α_{wf} is the specific absorptivity of water in the film, and γ_f is an optical constant

$$\gamma_f \equiv \frac{2\pi n_p}{\lambda}\left(\sin^2\theta - \left(\frac{n_f}{n_p}\right)^2\right)^{1/2} \quad (2)$$

where λ is the wavelength in vacuo, θ is the incident angle at the plate–film interface ($\theta = 45°$, here), and n_p and n_f are the refractive indices of the plate and film, respectively. For the purposes of this calculation, we will take the average wavenumber $1/\bar{\lambda} = 3400\ cm^{-1}$, from which $\bar{\lambda} = 2.94\ \mu m$. We will ignore dispersion (wavelength dependence) of the refractive index, especially since we used integrated absorbances over a wide wavelength range, over which dispersion effects may average out. Then, $n_p \simeq 4.02$ and $n_f = 1.50$, from which we get $\gamma_f = 5.16\ \mu m^{-1}$. We also ignore changes in the refractive index of the film after water entry. The results are not sensitive to such changes.

The thickness of the LB film was estimated to be $l = 0.29\ \mu m$ ($= 119 \times 0.0049/2\ \mu m$). The average spacing per bilayer (49 Å) was determined from the X-ray spacing of a 10-bilayer calcium stearate film. (In this experiment seven lines were observed in the ratio 1, 1/2, 1/3, 1/4, 1/5, 1/6, and 1/7).

The absorptivity α_{wf} is a combined measure of the specific material absorptivity, the angle of incidence, and the number of reflections. It was estimated from the absorbance of a bulk water layer on the same plate under identical conditions: $A_B = 349\ cm^{-1}$. Here,

$$A_B = \int_0^{\infty} \rho_{ww}\alpha_{ww} e^{-2\gamma_w x}\, dx = \frac{\rho_{ww}\alpha_{ww}}{2\gamma_w} \quad (3)$$

where ρ_{ww} is the molar density of bulk water ($55.5\ mol \cdot L^{-1}$), α_{ww} is the absorptivity of water in a bulk water phase, and

$$\gamma_w = \frac{2\pi n_p}{\lambda}\left(\sin^2\theta - \left(\frac{n_w}{n_p}\right)^2\right)^{1/2} \quad (4)$$

The parameters n_p, λ, and θ have been defined, and n_w is the refractive index of water, $n_w = 1.33$. Then $\gamma_w = 5.36\ \mu m^{-1}$, and $\alpha_{ww} = 67.4\ L \cdot mol^{-1} \cdot \mu m^{-1} \cdot cm^{-1}$.

Equations 1 and 3 yield

$$\rho_{wf}^{\circ} = \rho_{ww}\frac{A_{H0}}{A_B}\frac{\alpha_{ww}}{\alpha_{wf}}\frac{\gamma_f}{\gamma_w}\left(\frac{1}{1 - e^{-2\gamma_f l}}\right) \quad (5)$$

If we assume that $\alpha_{wf} \simeq \alpha_{ww}$, then we get $\rho_{wf}^{\circ} = 1.59\ mol \cdot L^{-1}$ for the film before contacting water, and $\rho_{wf}^{f} = 0.70$ mol L^{-1} after the water was removed. Because the film was thick, the density ratio here is about equal to the absorbance ratio. Using a density estimate of $1\ g \cdot cm^{-3}$ for the film, we find water contents of 2.7 and 1.26 wt %, or roughly one water molecule per calcium ion (and one molecule per two calcium ions after water exposure).

Having estimated the water content, we will now consider the film microstructure before and after the water exposure. In the CH_3 ν_a stretching region (Figure 2), the out-of-plane CH_3 ν_a vibration cannot be seen. Peak 3 is visible, but its location ($\sim 2945\ cm^{-1}$) does not correspond to any major CH vibration. Either it is the CH_2 ν_a vibration next to the carboxylate group[11] or it is an overtone of the COO^- ν vibration at 1550 or 1420 cm^{-1}, since the peak can no longer be resolved upon reaction of the COO^- to form COOH. The CH_2 ν bands, 5 and 9, are located at 2918 and 2850 cm^{-1} respectively, which are characteristic of a trans chain conformation.[12] The CH_3 ν_s peak, 7, is barely discernible in the 0° spectrum but is much more pronounced in the 90° spectrum, because the CH_3 ν_s vibration in a LB film has a large component perpendicular to the crystal surface. Moreover, the electric field in ATR at 0° polarization has only a y component (across the width of the crystal surface), while at 90° polarization it has components in the x and z directions (along the length and normal to the crystal surface). Hence, dipole components normal to the crystal surface only give rise to peaks in spectra at 90° polarization. Since, there were no visible changes in the CH region after the water exposure, we inferred that the crystallinity and orientation of the film were unaffected by the water contact and the subsequent drying. Figure 2C shows the carboxylate stretch and the CH_2 deformation region. There is a peak at 1620 cm^{-1} due to the O–H deformation vibration of the hydration water. The carboxylate ion stretching bands, 11 and 13, are split into distinct doublets. This splitting is most likely due to the water of hydration, as dehydration causes the doublets to form singlets (section 3.4). The smaller peak intensity of the ν_s compared to the ν_a vibration arises from the differences in the values of their dynamic dipole moments.

The CH_2 δ band, 12, is split into a doublet, indicating that there are two molecules per unit subcell associated with the chain packing.[13-15] Band 12 seems to overlap

(8) Harrick, N. J. *Internal Reflection Spectroscopy*; Interscience: New York, 1967.
(9) Mirabella, F. M., Jr. *Appl. Spectrosc. Rev.* **1985**, *21*, 45.
(10) Stratton, J. A. *Electromagnetic Theory*; McGraw-Hill: New York, 1941; pp 497–500.
(11) Bellamy, L. J. *The Infrared Spectra of Complex Molecules*; Wiley: New York, 1975.
(12) Snyder, R. G.; Strauss, H. L.; Elliger, C. A. *J. Phys. Chem.* **1982**, *86*, 5145.
(13) Colthup, N. B.; Daly, L. H.; Wiberly, S. E. *Introduction to Infrared and Raman Spectroscopy*, 3rd ed.; Academic Press: New York, 1990.
(14) Snyder, R. G. *J. Mol. Spectrosc.* **1960**, *4*, 411.

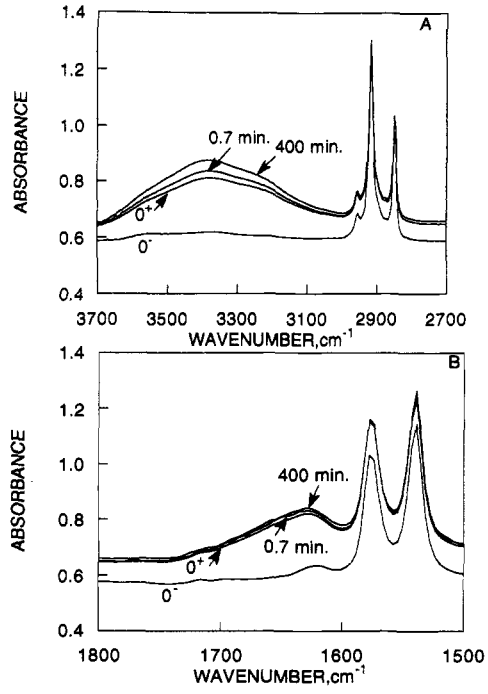

Figure 3. Unpolarized ATR spectra of 119-layer LB film of $CaSt_2$ on Ge during exposure to water on top of it at 25 °C: 0⁻, initial spectrum; 0⁺ immediately (~5 s) after exposure.

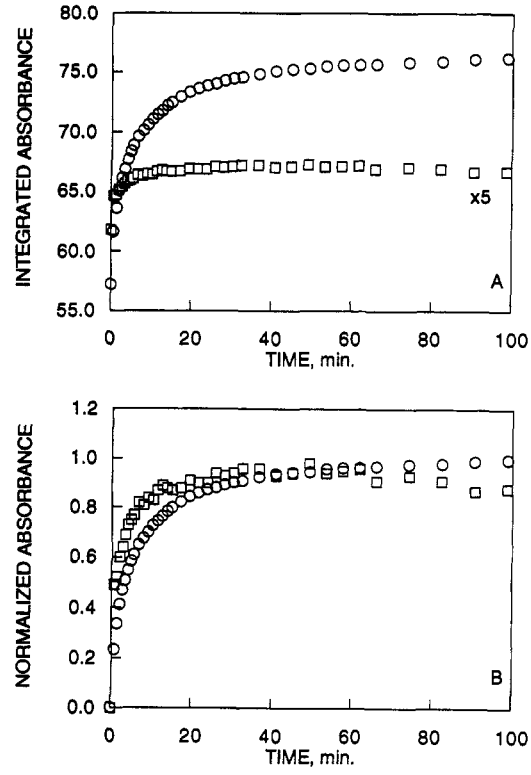

Figure 4. Integrated absorbance (cm^{-1}) of water peaks (A) and normalized absorbance (B): ○, area from 3800 to 3000 cm^{-1}; □, area from 1750 to 1550 cm^{-1}. All peaks due to film were subtracted prior to integration.

with another band which obscures the splitting. The structure has been assigned to an orthorhombic crystal lattice.[6] The CH_2 ($\gamma + \omega$) progression band appears from 1380 to 1180 cm^{-1}. This band is associated with methylene chains comprised of an all trans conformation. Overall, the water exposure caused no changes in either the CH_2 δ or the ($\omega + \gamma$) bands, which are sensitive to the crystal structure and chain conformation, thus, supporting the conclusion that water contact and penetration does not alter the film structure.

Peak 16 (for which we have no definite assignment) disappears after the conversion of COO^- to COOH, while the film is dehydrated. This leads us to speculate that the band is associated with a deformation vibration of the carboxylate ion or with an OH deformation in the hydration water. The O–C–O linkage does display an absorption band in this region. Peak 17 is possibly due to a C–C vibration. Peak 19 is assigned to the CH_2 r (in phase) vibration of the methylene chain. It appears in most hydrocarbons with at least four carbons,[11] and its splitting supports the inference of an orthorhombic structure for LB films of $CaSt_2$.[6]

The high-resolution spectra and the dichroic ratios before and after the LB film was contacted with water show no compositional, structural, or conformational changes within the film. In addition, there was no significant loss or dissolution of the film. The water uptake caused no discernible changes in the film structure, which suggests that the water was not incorporated in the crystal, but rather filled gaps or holes or defects in the film.

3.2. Water Uptake Dynamics. We now consider the rate of absorption of water by the film. Examples of the transient spectra collected during the water uptake are given in Figure 3. The two bands of interest are the OH stretching region (aroung 3400 cm^{-1}) and the OH deformation band at about 1620 cm^{-1}. The large jump in water peak at $t = 0^+$ occurs in part because the evanescent IR wave extends beyond the film and interacts with the water present on top of the LB film. The signal gradually increases with time as water is taken up into the film, increasing the amount of water probed by the evanescent wave. The penetration length of the 1620-cm^{-1} band is approximately twice that of the 3400-cm^{-1} band. Hence, at 1620 cm^{-1} a larger fraction of the total water signal originates from the water on top of the film, compared to the case for the higher frequency band. This leads to much smaller changes in the 1620-cm^{-1} band, limiting its use for measuring water transport into the film. This is demonstrated by the results for the integration of the water bands (Figure 4). The area of the 3400-cm^{-1} band increases by ca. 35%, whereas the area of the other band increases by ca. 10%. Nonetheless, when the normalized absorbance $(A - A_{intial})/(A_{final} - A_{initial})$ was plotted against time, for both bands the time scale for equilibration was about the same.

The first spectrum ($t = 0^+$) was obtained within about 2 s after the water filled the space above the film. Together, the filling process and the first spectrum took less than 5 s. We assign the first spectrum at 5 s. The question is whether the first measurement truly corresponds to water on top of the previous hydrated film without any appreciable water penetration. For that configuration, the expected absorbance would have been as follows:

$$A_0 = A_{H0} + A_{WATER} \tag{6}$$

where A_{H0} is given by eq 1 and

$$A_{WATER} = \rho_{ww}\alpha_{ww}e^{-2\gamma_w l}\int_l^\infty e^{-2\gamma_w(x-l)}\,dx = \frac{\rho_{ww}\alpha_{ww}}{2\gamma_w}e^{-2\gamma_w l} \tag{7}$$

The expected integrated absorbance before any water penetration is, therefore

$$A_0 = 9.5 + 349e^{-2\cdot5.16\cdot0.29} = 27\ cm^{-1}$$

This value is a lot less than the first absorbance mea-

(15) Broadhurst, M. G. *J. Res. Natl. Bur. Stand.* **1962**, *A66*, 241.

surement A_{f0} = 57.2 cm^{-1} (Figure 4), which would correspond to a much thinner film of l = 0.193 μm, or 16.2 Å per layer, or 32.4 Å per bilayer. This possibility is unlikely, because the interbilayer distance was measured to be about 49 Å for a similar film. A more likely explanation for the difference between A_0 and A_{f0} is that some water invaded the film during the first few seconds of contact. If the film had a significant volume fraction of defects, pinholes, or grain boundaries, which were filled instantly (in less than 5 s), the first measurement would provide a measure of the new water density in the film, ρ_{wf0}, if it is uniform. Then

$$A_{f0} = \frac{\rho_{wfo}\alpha_{wf}}{2\gamma_f}(1 - e^{-2\gamma_f l}) + \frac{\rho_{ww}\alpha_{ww}}{2\gamma_w} e^{-2\gamma_f l} \quad (8)$$

With this scheme, one would get ρ_{wf0} = 6.6 mol·L^{-1}, or about 11 wt % water. If this amount of water had swelled or hydrated the calcium stearate crystal, then the spectrum of the surfactant should have changed. Since the spectrum of the stearate remained the same, and the water band looks the same as that bulklike water, we postulate that the additional water was bulk water. We caution that this inference is tentative, because of some uncertainty about the precise thickness l.

Irrespective of this uncertainty, it is clear that the film took on additional water, since the absorbance at long times increased to $A_f(\infty)$ = 75.9 cm^{-1}. The additional water is about [(75.9–57.2)/9.5] × 2.7 = 5.3 wt %. Thus, the film contained at equilibrium (steady state) at least 8 wt % water and probably as much as 16 wt % (based on the above scheme). This LB film could hardly qualify as a barrier material for water, but instead it has to be thought as a porous, water-absorbing structure.

The rate at which the absorbance at 3400 cm^{-1} increases (Figure 4) can be used as a basis for estimating the transport rate of water. A preliminary estimate of an apparent diffusion coefficient, based on the assumption of a one-dimensional Fickian diffusion mechanism through a thickness l, yields $D_{app} \simeq l^2/t^*$, where t^* is the equilibration time, $t^* \simeq$ 50 min. Then $D_{app} \simeq 3 \times 10^{-13}$ cm^2 s^{-1}. This value is surprisingly low by comparison to other values for organic membranes, especially if one considers that the absorbance increases extremely fast at the beginning and the film material takes up a large amount of water. The low value is probably due to the low permeability of water through hydrocarbon regions.

A more precise interpretation of the data is as follows. The time-dependent absorbance is

$$A(t) = \alpha_{wf}\int_0^l \rho_{wf}(x,t)e^{-2\gamma_f x}\,dx + \frac{\alpha_{ww}\rho_{ww}}{2\gamma_w} e^{-2\gamma_f l} \quad (9)$$

where $\rho_{wf}(x,t)$ is the time-dependent molar density in the film. The quantity $\rho_{wf}(x,t)$ is assumed to be described by Fick's second law with a diffusion coefficient D_{app}, and the following boundary/initial conditions

$$\rho_{wf}(l,t) = \rho_{wf}^{\infty} \quad (10)$$

which reflects the partitioning of water at the water/film interface and provides the final water concentration throughout the film; also

$$\frac{\partial \rho_{wf}}{\partial x}(0,t) = 0 \quad (11)$$

which reflects that the ATR plate is not penetrated by water, and

$$\rho_{wf}(x,0) = \rho_{wf}^{\circ} \quad (12)$$

(Notice that $\rho_{ww}^{\circ} \neq \rho_{wf0}$.) The solution to this transport problem, along with eq 9, can be used to estimate the value of the apparent diffusion coefficient. Calculation details are omitted. Using the initial film density ρ_{wf}° = 1.59 mol·L^{-1} and the final film density ρ_{wf}^{∞} = 9.37 mol·L^{-1}, as estimated before, we have plotted in Figure 5 the expected absorbance for various values of D_{app}, based on eq 9. One can see that the value of D_{app} which matches the absorbance at each instant decreases with time, from ca. 10^{-10} to ca. 5×10^{-13} cm^2·s^{-1}.

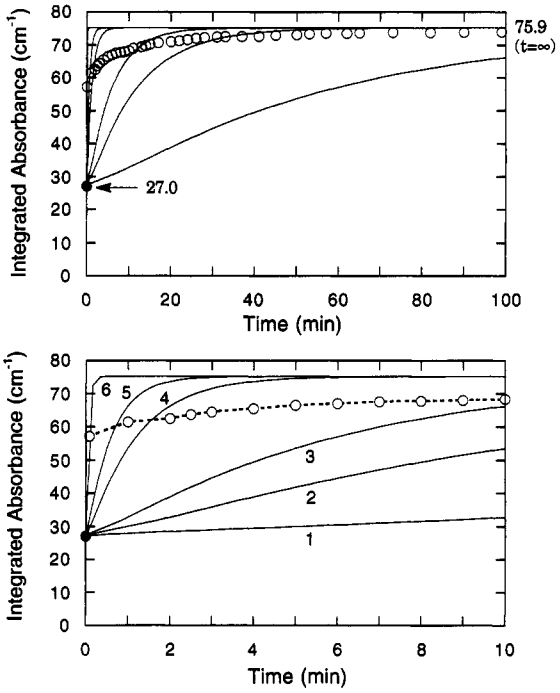

Figure 5. Comparison of measured integrated absorbances of water (at 3000–3800 cm^{-1}) from Figure 4A to calculated absorbances based on eq 9, with a one-dimensional diffusion model with an apparent diffusion coefficient D_{app} = 10^{-10} cm^2·s^{-1} (6), 10^{-11} (5), 5×10^{-12} (4), 10^{-12} (3), 5×10^{-13} (2), and 10^{-13} (1).

The results suggest that the mechanism of water transport is not purely diffusive. Instead, the following picture emerges. A significant fraction of the absorbed water penetrates the film rapidly, probably through highly permeable regions, or film defects, or pinholes. Then, the water reaches other domains, either via flow in pores or via diffusion, but in directions both normal to the film and laterally. For lateral transport, the effective diffusion length of the film would not be equal to the film thickness and would need to be determined independently. Then, of course, the true material diffusion coefficient D could be quite different from the values of the apparent diffusion coefficient reported above. One would need a more detailed two-dimensional description of the diffusion path to estimate diffusivity which could also be anisotropic in a well-ordered material.

3.3. Film Microstructure before and after Ion Exchange. We have done ion exchange experiments as follows. An HCl/H_2O solution of pH = 3.0 was placed on 29-layer (l = 0.072 μm) calcium stearate LB film. Prior to and after the ion exchange of calcium by protons, high resolution spectra were collected at s- and p-polarizations of the infrared beam: p is parallel to the plane of incidence and normal to the surface (90°); s is normal to the plane of incidence and parallel to the surface (0°) (Figure 6 and Table I). These spectra indicate significant compositional and structural changes upon ion exchange. After the film was converted to StH, it appears to be essentially anhydrous (no peak at 3380 cm^{-1}, even though it had been

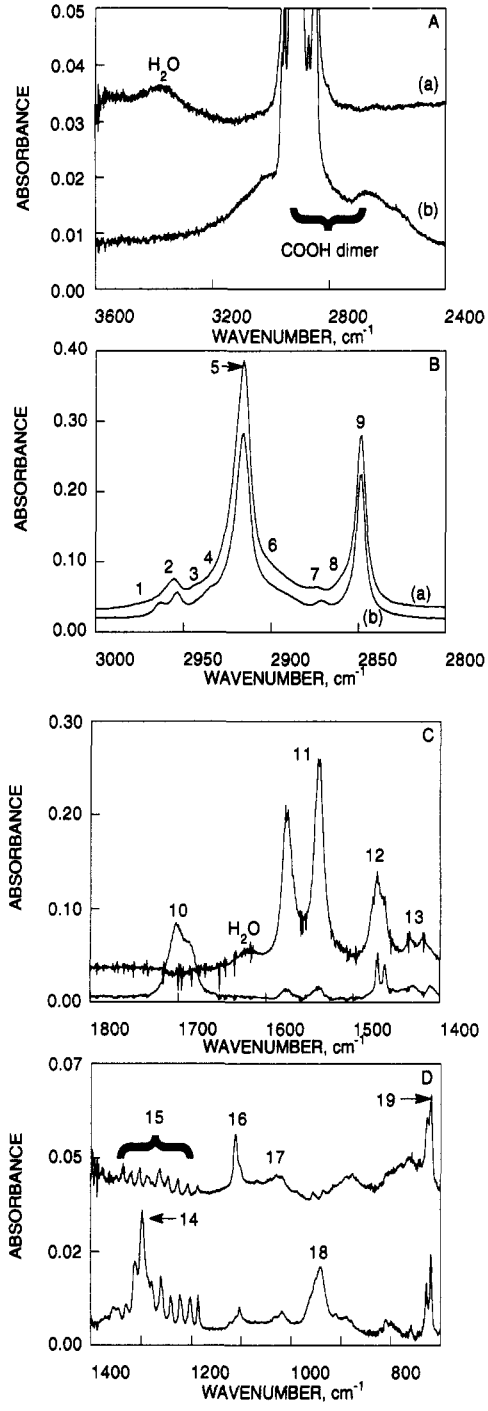

Figure 6. ATR-FTIR spectra of 29 layers of $CaSt_2$ on Ge crystal at 90° polarization (a) initially and (b) after ion exchange: pH = 3 HCl/H_2O; 1 cm^{-1} resolution; 45° angle of incidence. Peaks are identified in Table I. A, B, C, and D are various spectral regions. The spectra at 0° polarization (not shown) are similar. The high-frequency noise in part C is due to water vapor in the spectrometer.

covered with aqueous solution just prior to the measurement. The water O–H deformation band at 1620 cm^{-1} was also lost after ion exchange. The Ca^{2+}/COO^- complex is evidently more capable of retaining water than the COOH group. One question that arises is as to the fate of the calcium originally in the LB film. The absence of water in StH indirectly suggests that no $CaCl_2$, which is highly hygroscopic and would have retained some water, was left in the film after the exchange process. $CaCl_2$ was probably dissolved into the acidic aqueous medium. The broad bands shown in Figure 6b at the base of the

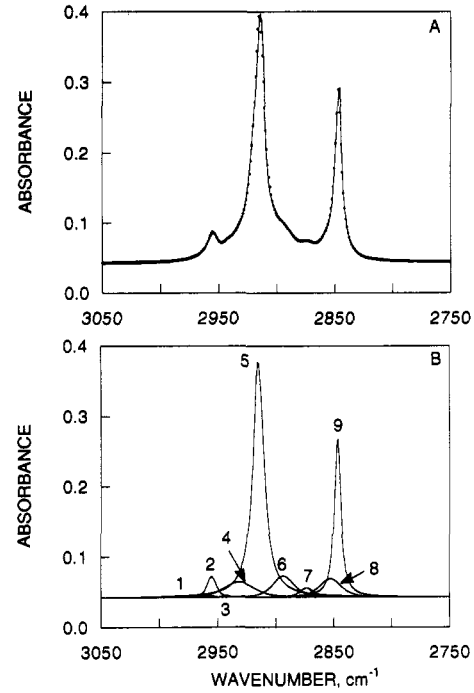

Figure 7. Curve fit of hydrocarbon stretch region A for spectrum a of Figure 6. Dots are overall fit; line is the spectrum. Individual curves are shown in B. Parameters values are given in Table II.

hydrocarbon stretching bands are characteristic of dimerized fatty acids.[11] The band which best shows the formation of the acid from the calcium salt is the C=O stretching vibration, 10, at 1700 cm^{-1}. Its frequency also suggests that it arises from an acid dimer[11] and consists of two overlapping peaks associated with a cis and trans configuration of the fatty acid dimer. A band, which is a deformation vibration of the entire O–C–O–H linkage, appears at 1300 cm^{-1}. The band is in the middle of the $CH_2(\omega + \gamma)$ progression band, which makes quantitative analysis of its intensity difficult. The final band, 18, which shows the formation of a fatty acid dimer, is located at 940 cm^{-1} and is assigned to an O–H out-of-plane deformation associated with the fatty acid ring-dimer.[11]

The conversion of the carboxylate to carbonyl is evident both from the increase in the carbonyl band intensity and from the decrease of the carboxylate bands intensities. Most of the film which was not contacted by the solution was removed (using a cotton swab, or a thin wooden rod) prior to collecting spectrum b, so that the extent of the reaction could be better estimated. Only a small fraction of COO^- remained in the final film, probably due to incomplete removal of noncontacted film. It is inferred that the reaction went to completion in the film that was contacted. Peak 16 appears to be associated with the carboxylate groups or to hydration water, as it disappears during the course of ion exchange. Its most likely assignment would be a deformation vibration of the COO^- group or the hydration OH bond, since alcohols have a C–O–H deformation band in this region.[13]

In addition to the chemical changes inferred from the vibrations of the polar carbonyl group, the various hydrocarbon bands show significant structural changes after ion exchange. To better quantify these changes, detailed spectral analyses were done, as demonstrated by the curve fits for the 90° spectra in Figure 7. For several such spectra (shown in ref 7), the resulting parameters are given in Table II. Peaks 5 and 9 were fit as purely Lorentzian, as their relatively large size allowed a safe determination of the peaks shapes. All other peaks were

Table II. Curve-Fit Parameters for 29-Layer $CaSt_2$ LB Film Exposed to HCl Solution

	peak	position (cm^{-1})	peak intensity	fwhm (cm^{-1})	area (cm^{-1})
0° (s-pol.)	1	2965	0.0061	21	0.17
before	2	2955	0.025	10	0.33
ion	3	2943	0.002	5	0.014
exchange	4	2932	0.022	28	0.82
	5	2915	0.32	11	5.6
	6	2893	0.028	20	0.76
	7	2876	0.01	18	0.24
	8	2853	0.026	22	0.74
	9	2847	0.22	6	2.3
0° (s-pol.)	1	2962	0.0078	9	0.097
after	2	2953	0.023	6	0.018
ion	3				
exchange	4	2932	0.022	27	0.78
	5	2915	0.23	10	3.5
	6	2894	0.026	28	0.98
	7	2869	0.011	8	0.12
	8	2852	0.015	20	0.39
	9	2847	0.019	6	1.7
90° (p-pol.)	1	2964	0.0045	16	0.093
before	2	2955	0.030	9	0.37
ion	3	2943	0.0035	6	0.026
exchange	4	2932	0.022	30	0.88
	5	2915	0.34	11	5.9
	6	2894	0.030	21	0.86
	7	2874	0.013	13	0.23
	8	2853	0.026	22	0.76
	9	2847	0.23	6	2.3
90° (p-pol.)	1	2962	0.016	9	0.19
after	2	2953	0.065	6	0.23
ion	3				
exchange	4	2932	0.026	24	0.83
	5	2915	0.25	10	3.9
	6	2894	0.028	28	1.0
	7	2870	0.012	8	0.12
	8	2852	0.016	23	0.48
	9	2847	0.020	6	1.8

fit with a fixed 50:50 Gaussian-to-Lorentzian shape, since using either lineshape produced about the same quality of fit.

In the 90° spectrum, only one CH_3 ν_a peak could be fit and clearly observed. While this band (not shown) cannot be distinguished in the initial 0° spectrum, in the 90° spectrum it is discernible, indicating that this vibration has a larger component of its dipole moment perpendicular to the crystal surface than parallel to it. After the ion exchange, both the in-plane and out-of-plane components of the CH_3 ν_a vibration are clearly observable in both the 0° and 90° spectra, because the peaks are narrower. Chain reorientation, inferred from the CH_2 stretching peaks (detailed later), could also have changed the intensity of the methyl bands. In the 0° and 90° spectra, the fwhm's were 9 and 6 cm^{-1}, respectively. The original single major peak had a fwhm of about 10 cm^{-1} and was located at 2955 cm^{-1}, which lies between the two resolved singlets at 2962 and 2953 cm^{-1}. Therefore, the peak in the initial spectrum is most likely a combination of both the in-plane and the out-of-plane CH_3 ν_a components, but these components could not be resolved due to their large widths. Narrowing of CH_3 ν_a band has been attributed to decreased mobility at the end of the hydrocarbon chain.[16] The ion exchange may have rendered the methyl group less mobile than in the initial film.

In addition to the changes in the methyl peaks, the methylene stretching bands also point to significant structural changes upon ion exchange. The initial dichroic ratios for the CH ν bands (peaks 5 and 9) were $D(\nu_a) = 0.95 \pm 0.02$ and $D(\nu_s) = 0.98 \pm 0.01$. After the ion exchange, they were $D(\nu_a) = 0.90 \pm 0.02$ and $D(\nu_s) = 0.95 \pm 0.01$. The dichroic ratio for a random orientation of this film would be 0.87, in the limit of small thickness ($\gamma_f l \ll 1$, here $\gamma_f l = 0.36$). The dichroic ratios show that there was a change in the orientation of the hydrocarbon chain with respect to the ATR surface. If the CH_2 chains had a uniaxial orientation around the surface normal (i.e. isotropic in the x–y plane), and since the CH_2 ν dipoles are normal to the chain axis, then, for a thin film the average angle $\bar{\gamma}_0$ of tilt of the chain from the surface normal is found as described previously.[17] Before the ion exchange and based on the ν_a vibration, one finds $\bar{\gamma}_0(\nu_a) = 43 \pm 4°$; based on the ν_s vibration, one finds $\bar{\gamma}_0(\nu_s) = 35 \pm 2°$. After ion exchange, the chain tilt angle was $\bar{\gamma}_0(\nu_a) = 50 \pm 4°$ or $\bar{\gamma}_0(\nu_s) = 41 \pm 2°$. If the film chains were truly uniaxially distributed with the same angle γ_0 for all chains, then the dichroic ratios, and hence the angles calculated for the two vibrations, should be equal. The areas of the symmetric bands are more precisely found, as they have fewer overlapping bands.

The width of the CH_2 ν_a band (5) is indicative of the mobility of the hydrocarbon chain.[18] Here, the widths for the 0° and 90° spectra decreased from 11.2 ± 0.3 and 11.2 ± 0.5 cm^{-1}, respectively, to 10.0 ± 0.1 and 10.0 ± 0.1 cm^{-1}. The slight narrowing of the bands indicates that after the ion exchange the hydrocarbon chains are less mobile. Peak 3 was not visible after the ion exchange and was not fit in the final spectra. The area ratio of bands 8 and 9 increased after ion exchange from 3.1 (0°) and 3.0 (90°) to 4.4 (0°) and 3.8 (90°). This loss of intensity upon reaction supports the tentative assignment of band 8 as a stretching vibration of the α-methylene.

The carbonyl stretching and methylene scissoring vibrations are seen in Figure 6C. Initially, no C=O signal was observed, since the film was pure $CaSt_2$. The carboxylate ν_a and ν_s bands are visible and labeled 11 and 13. In the initial spectrum, the dichroic ratio for the carboxylate ν_a band is $5.8/5.9 = 0.98 \pm 0.02$. If the dipole moment were normal to the chain axis, then the average chain tilt angle of $\bar{\gamma}_0$ would be $35 \pm 3°$. This agrees well with the angle of $35 \pm 1°$ calculated using the CH_2 ν_s band, which has a dipole moment normal to the chain axis. The dipole moment of the COO^- asymmetric stretch is exactly perpendicular to the chain axis for one specific configuration, in which the line connecting the two oxygen atoms is perpendicular to the backbone plane, as a molecular model reveals. Should the COO^- lie in the plane of the backbone, then the asymmetric vibration dipole would be perpendicular to the last C–C bond or at an angle of 65° with respect to the chain axis. For this configuration, the angle γ_0 would be $26 \pm 6°$. In the stearic acid film, the dichroic ratio of the C=O vibration was $D = 2.20/2.30 = 0.96 \pm 0.02$. If the C=O bond were normal to the chain axis, then $\bar{\gamma}_0 = 40 \pm 3°$, which agrees well with the value of 42° deduced from the dichroic ratio of the CH_2 ν_a vibration.

The CH_2 δ vibration (12) of $CaSt_2$ is a slightly split doublet in the 90° spectrum (and a bit more clearly split in the 0° spectrum).[13-15,19] By contrast, the ion exchanged film displays a well-split doublet. The narrower peaks suggest that the stearic acid is more highly crystalline than the initial $CaSt_2$. Additional evidence for structural changes is provided by the progression band (15), which

(16) MacPhail, R. A.; Snyder, R. G.; Strauss, H. L. *J. Chem. Phys.* **1982**, *77*, 1118.

(17) Ahn, D. J.; Franses, E. I. *J. Phys. Chem.* **1992**, *96*, 9952.

(18) Wood, K. A.; Snyder, R. G.; Strauss, H. L. *J. Chem. Phys.* **1989**, *91*, 5255.

(19) Rabolt, J. F.; Burns, F. C.; Schlotter, N. E.; Swalen, J. D. *J. Chem. Phys.* **1983**, *78*, 946.

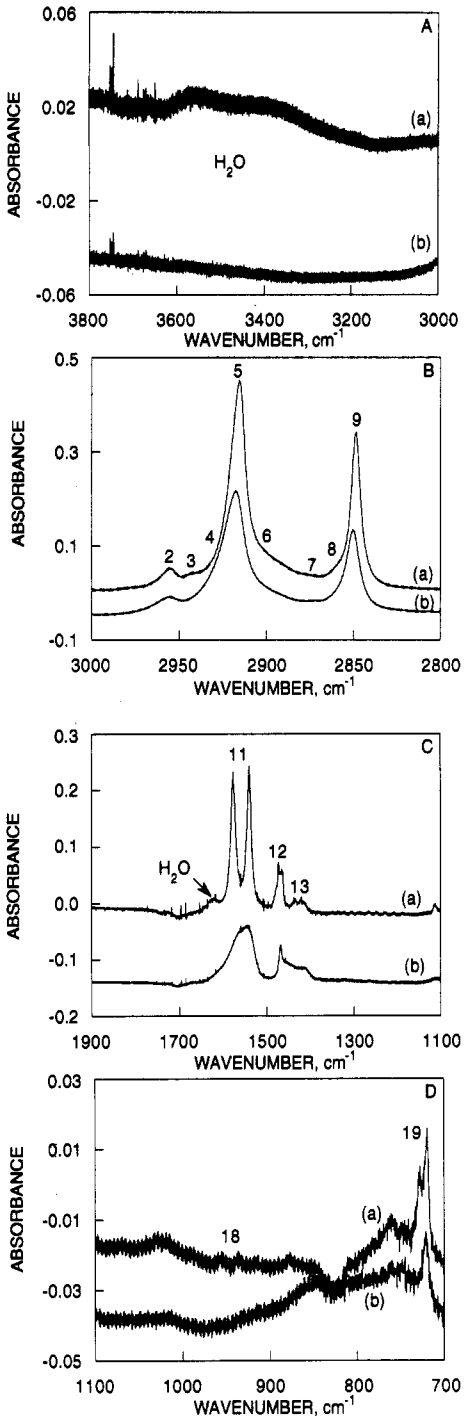

Figure 8. ATR-FTIR spectra of 29-layer LB film of $CaSt_2$ on Ge at 0° polarization initially (a) and after heating to 136 °C and cooling to 25 °C (b): 1 cm^{-1} resolution; 45° angle of incidence. Peaks are identified in Table I. A, B, C, and D are various spectral regions.

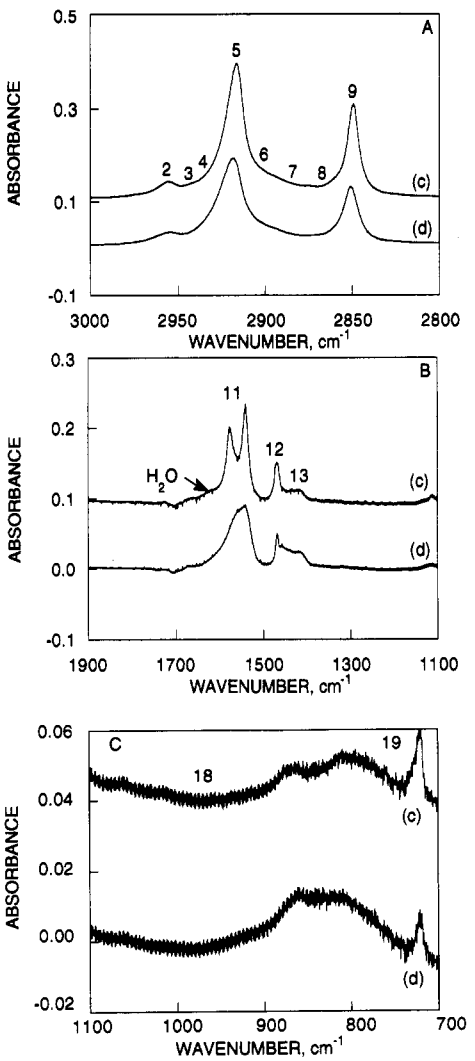

Figure 9. Same as Figure 8, except spectrum c is spectrum b of Figure 8 after aging in ambient condition for 2 days and spectrum d is spectrum c after being reheated to 136 °C and cooled to 25 °C.

has a larger intensity in the acid film. Since these bands dipole moments are parallel to the chain axis, the intensity is higher in the 90° spectra than in the 0° spectra. Senak *et al* proposed a simple model for evaluating changes in the progression band intensity due to the introduction of gauche rotamers in the chain.[20] A small reduction in the number of gauche conformations per chain would dramatically increase after ion exchange the intensity of the progression band (Figure 6D). The positions of the progression peaks of the StH agree with those of Hayashi and Umemura,[21] who assigned them to a cis isomer of the COOH dimer. The $CaSt_2$ bands also are observed in the same locations reported by Kimura et al.[6]

The final band of interest (19) is the totally in-phase rocking band CH_2 r. In the $CaSt_2$ film, the two peaks at 728 and 720 cm^{-1} can barely be resolved. After the conversion to StH, peak narrowing allows the two components to be easily resolved. This narrowing could be the result of loss of mobility of the hydrocarbon chains, as also inferred by the methyl and methylene stretches, or of increase in crystallinity.

3.4. Effect of Annealing on Microstructure. A 29-layer $CaSt_2$ film was first heated at 136 °C for 20 min, then kept at ambient conditions for 2 days, and finally reheated at 136 °C and recooled prior to ion exchange. ATR spectra (0° and 90° polarized) were collected at each stage of the heat treatment. Only the 0° spectra are presented here (Figures 8 and 9). The hydrocarbon stretch regions were fit as previously described, and the curve fit parameters are given in Tables III and IV. The film appears to have become nearly anhydrous after heating at 136 °C (Figure 8A,C). The CH_2 stretch peaks were broadened and moved to higher frequencies, implying that the crystal structure and chain conformation were changed. The COO^- ν_a peak

(20) Senak, L.; Moore, D.; Mendelsohn, R. *J. Phys. Chem.* **1992**, *96*, 2749.

(21) Hayashi, S.; Umemura, J. *J. Chem. Phys.* **1975**, *63*, 1732.

Table III. Curve-Fit Parameters 0° Polarization for 136 °C Treatment

	peak	position (cm^{-1})	peak intensity	fwhm (cm^{-1})	area (cm^{-1})
initial	1	2965	0.0058	18	0.13
	2	2957	0.034	10	0.44
	5	2918	0.432	11	7.2
	7	2878	0.245	25	0.79
	9	2852	0.321	6	3.16
136 °C	1	2971	0.0030	17	0.07
	2	2958	0.027	16	0.58
	5	2920	0.244	14	5.27
	7	2964	0.017	26	0.56
	9	2853	0.165	9	2.27
136 °C	1	2974	0.0037	15	0.07
aged for	2	2958	0.030	15	0.60
2 days	5	2919	0.290	12	5.53
	7	2871	0.019	36	0.88
	9	2852	0.204	8	2.47
136 °C	1	2969	0.0026	22	0.077
after	2	2957	0.018	17	0.39
aging	5	2921	0.173	15	4.01
	7	2865	0.010	25	0.34
	9	2854	0.116	10	1.76
after ion	1	2964	0.0060	8	0.06
exchange	2	2956	0.019	6	0.14
	5	2918	0.190	9	2.75
	7	2874	0.0089	8	0.01
	9	2852	0.167	6	1.46

Table IV. Curve-Fit Parameters 90° Polarization for 136 °C Treatment

	peak	position (cm^{-1})	peak intensity	fwhm (cm^{-1})	area (cm^{-1})
initial	1	2966	0.0087	21	0.24
	2	2957	0.036	10	0.49
	5	2918	0.462	10	7.60
	7	2882	0.023	22	0.67
	9	2852	0.313	6	3.10
136 °C	1	2968	0.0062	20	0.16
	2	2958	0.030	16	0.61
	5	2920	0.261	14	5.81
	7	2872	0.018	35	0.85
	9	2853	0.181	9	2.57
136 °C	1	2970	0.0044	19	0.11
aged for	2	2958	0.031	16	0.67
2 days	5	2920	0.260	14	5.77
	7	2869	0.018	32	0.78
	9	2853	0.180	9	2.53
136 °C	1	2971	0.0029	19	0.08
after	2	2958	0.022	17	0.50
aging	5	2921	0.191	15	4.49
	7	2867	0.013	28	0.48
	9	2854	0.132	10	1.98
after ion	1	2964	0.017	8	0.18
exchange	2	2955	0.025	6	0.20
	5	2918	0.235	9	3.31
	7	2874	0.012	8	0.13
	9	2852	0.016	20	0.43

has broadened, and its center lies between the two original doublets. Heating at 120 °C resulted in dehydration and in the formation of a near singlet COO^- band, at the same position as the low-frequency component of the doublet,[7] but the CH_2 bands remained unchanged. It appears that the crystal structure was altered at 136 °C, but not at 120 °C or lower temperatures.

The CH_2 δ vibration shows no crystal splitting, indicating either that the film is amorphous or that it contains one molecule per unit cell.[13-15] The CH_2 ($\gamma + \omega$) progression band cannot be seen in the spectrum of the annealed film. Thus, the number of gauche bonds or defects introduced by the heating eliminated nearly all trans conformations of the hydrocarbon chains. The CH_2 totally in-phase rocking band, which was originally split, became a singlet after heating. The singlet is characteristic of amorphous hydrocarbon chains.[11] The primary feature in the hydrocarbon region is the additional loss of material due to the heating. After the final annealing the film retained approximately 63% of its original CH signal.

Table V. Dichroic Ratios and Average Chain Tilt Angle for a 29-Layer $CaSt_2$ LB Film after Various Treatments

conditions	$D(\nu_a)$	$D(\nu_s)$	$\bar{\gamma}_0$ (ν_a) (deg)	$\bar{\gamma}_0$ (ν_s) (deg)
initially	0.95	1.02	41	26
after 136 °C	0.91	0.88	49	54
after 2 days at ambient	0.96	0.97	40	38
after 136 °C again	0.89	0.89	52	52
after ion exchange	0.83	0.90	62	50

In the spectra collected after the annealed film was kept for 2 days at ambient conditions (Figure 9c), the film was rehydrated, and the COO^- band was split again. After 30 additional minutes of annealing at 136 °C (Figure 9d), the film was again dehydrated, with no splitting of the COO^- band.

Table V gives the dichroic ratios and the average chain tilt angles for the various heat treatments. The values for the ν_s band are the more precise, as this band overlaps with fewer other bands. The chain tilt angles $\bar{\gamma}_0$ calculated for the original film agree with those of the previous $CaSt_2$ films studied. After heating at 136 °C, $\bar{\gamma}_0$ increased (based on data with either band). The value of 54° calculated from the CH_2 ν_s band is within 1° of the so-called "magic angle" of 54.7°, which also can indicate an effectively randomly oriented material.[17]

After being exposed to ambient laboratory conditions for 2 days, the calculated average tilt angle dropped to ~39°. Apparently, there was a rearrangement of the film after it had been exposed to humid conditions. The close agreement of the two $\bar{\gamma}_0$ values suggests that the film is closer to having uniaxial orientation than the initial film.[17] The average tilt angle $\bar{\gamma}_0(\nu_a)$ is consistently higher than $\bar{\gamma}_0(\nu_s)$ for untreated $CaSt_2$ films.

Upon reannealing of the film, the values of $\bar{\gamma}_0$ based on both bands increased to 52°, which is essentially identical to $\bar{\gamma}_0$ of an amorphous film (i.e., $\bar{\gamma}_0$ = 54.7°). After ion exchange the dichroic ratio for the CH_2 ν_a band dropped, while the ν_s value was essentially unchanged. This suggests that there was a rearrangement accompanying the ion exchange which resulted in the formation of a nonuniaxial structure.

Figure 10 shows the 0° and 90° spectra collected after the ion exchange of the annealed $CaSt_2$ film. These spectra are similar to the spectra obtained from ion-exchanged films which were not annealed. Thus, with initially a nearly amorphous film, the ion exchange produced a film that is as crystalline as a nonannealed ion-exchanged film. The implications to ion exchange dynamics will be discussed in a future communication.

The results show that LB films are poor barriers to water and acid solutions. Contact of the films with water indicates substantial and fast penetration, followed by slower diffusion-type absorption of water in the film structure. The hydration water content is small, but the overall bulk water content is high, revealing a large volume fraction of voids and defects. Another type of evidence is needed to determine whether all these voids or defects are initially present in the films or are induced in part by the water contact. Moreover, whereas the film microstructure does not change appreciably during the water contact, it changes drastically upon ion exchange or after

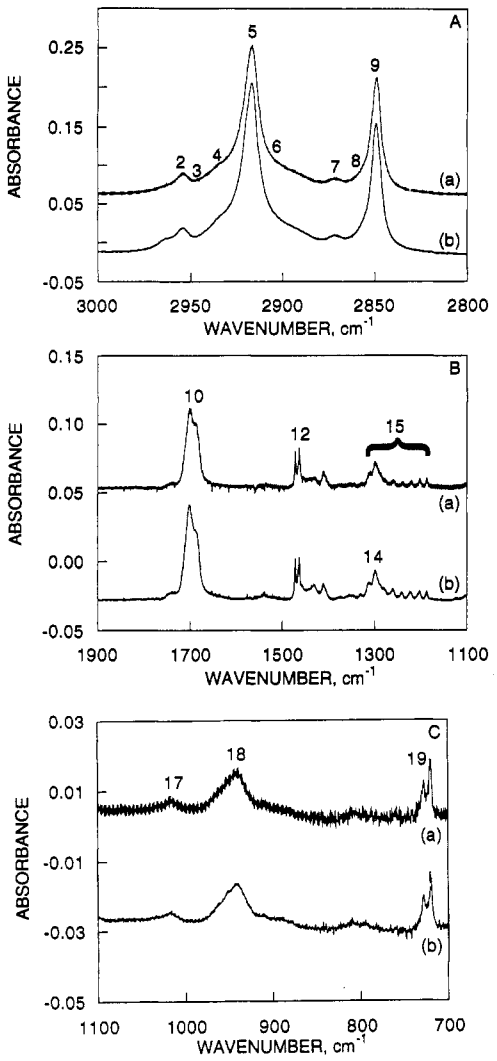

Figure 10. ATR-FTIR spectra of sample in Figure 8d after exposure to pH = 3 HCl/H_2O, at 0° polarization (a) and 90° polarization (b). A, B, and C are various spectral regions.

annealing at 136 °C. This temperature provides an upper limit of the operating range of these materials. To increase this range, different molecular structures or polymers may be needed. Finally, ion exchange of $CaSt_2$ films can be complete under favorable pH conditions.

4. Conclusions

Calcium stearate LB films are in a nearly all-trans conformation in an orthorhombic crystal packing and retain about 3 wt % water of hydration after LB deposition. Contact with water introduces an additional 13 wt % water but leaves the structure intact. The smallest apparent diffusion coefficient (that fits the long-time data) is about 3×10^{-13} cm^2/s^{-1}, taking about 50 min for a 3000 Å thick film to equilibrate. This minute diffusion coefficient, and the range of diffusion coefficients obtained from the model, may imply that certain regions in the film are not easily accessible and that it takes them longer to equilibrate with water than for water to penetrate more accessible regions of the film. A Fickian diffusion model and a one-dimensional water transport cannot describe the water uptake dynamics.

Although annealing of the film at 120 °C affects little the structure, annealing at 136 °C makes the film amorphous. The film subsequently recrystallizes as it is being rehydrated. Contact of the film with aqueous hydrochloric acid induces ion exchange to stearic acid, with no water of hydration, and recrystallization to a more ordered crystalline structure. Finally, ion exchange of an annealed and amorphous $CaSt_2$ film produces a film of StH which is quite crystalline and in fact similar in structure to a StH film produced from nonannealed crystalline $CaSt_2$ films. These results may be useful for the potential applications of LB films as membranes and materials for ion exchange.

Acknowledgment. This work was supported in part by two NSF equipment grants (CBT 864904 and CTS 9004147) and by David Ross Fellowships to D.J.A. and T.L.M. We thank Professor W. N. Delgass and Mr. G. J. Howsmon, from Purdue Univesity, for the use of their programs for fitting the FTIR spectra. We are also grateful to Mr. Peter Sutandar for doing some of the calculations reported on Figure 5.